Biodegradable nanoparticles exposing a short antiFLT1 peptide as antiangiogenic platform to complement docetaxel anticancer activity

Claudia Conte,[a,‖] Francesca Moret,[b,‖] Diletta Esposito,[a] Giovanni Dal Poggetto,[c] Concetta Avitabile,[d] Francesca Ungaro,[a] Alessandra Romanelli,[d,e] Paola Laurienzo,[c] Elena Reddi,[b,*] and Fabiana Quaglia [a,*]

[a] Department of Pharmacy, University of Napoli Federico II, Italy

[b] Department of Biology, University of Padova, Italy

[c] Institute for Polymers, Composites and Biomaterials, CNR, Pozzuoli (Napoli), Italy;

[d] Institute of Biostructure and Bioimaging, CNR, Napoli, Italy

[e] Department of Pharmaceutical Sciences, University of Milan, Italy

AUTHOR INFORMATION

Corresponding Author

* E-mail: quaglia@unina.it; elena.reddi@unipd.it

ABSTRACT

Inhibition of tumor angiogenesis is considered as a valuable clinical strategy to treat some tumors, although benefits in term of progression-free and overall survival have been modest. Recent findings have pushed toward the use of antiangiogenic drugs in combination with chemotherapy regimens to potentiate therapeutic outcome. Herein, we propose a novel type of biodegradable antiangiogenic core-shell polymeric nanoparticles (NPs) for the delivery of poorly water-soluble chemotherapeutics. An amphiphilic diblock copolymer of poly(ethyleneglycol)-poly(ε-caprolactone) (PEG-PCL) was conjugated with an anti-FLT1 hexapeptide (aFLT1) at -OH PEG end, mixed in appropriate ratios with a monomethoxy-PEG-PCL and nanoprecipitated to form core-shell aFLT1-bearing NPs (DBL_{aFLT1}). DBL_{aFLT1} were < 100 nm, exposed aFLT1 on the surface and showed a higher thickness of the external hydrophilic shell as compared to NPs that do not bear aFLT1 (DBL). Very interestingly, DBL_{aFLT1} showed an antiangiogenic activity in the human umbilical endothelial cells (HUVEC) tube formation assay three-fold higher than an equivalent dose of free aFLT1. To provide a proof-of-concept of DBL_{aFLT1} potential in the delivery of conventional chemotherapeutics, docetaxel (DTX) was selected as model drug. DBL_{aFLT1} entrapped DTX with high efficiency and sustained its release along time in simulated biological conditions. At a non-cytotoxic dose, DTX-loaded DBL_{aFLT1} almost completely abolished tube formation in HUVEC while inhibition of DTX loaded DBL was significantly lower. The cytotoxicity of DTX-loaded NPs in HUVEC and triple negative breast cancer cells (MDA-MB-231) was not significantly different from that of the free drug in a wide range of concentrations and up to 72 h. Studies carried out in MDA-MB-231 cells implanted in chicken embryo chorioallantoic

membranes (CAMs) evidenced an antiangiogenic activity of DTX-loaded DBL_{aFLT1} higher as compared with that of both DTX-loaded DBL and free DTX. While cancer cell migration from the tumor site was unaffected, the anticancer activity of DTX-loaded NPs was higher than that of free DTX and maximized for DTX-DBL_{aFLT1}. In perspective, these results suggest that the delivery approach proposed here can be applied to other lipophilic chemotherapeutics devoid of relevant antiangiogenic properties to improve the final therapeutic response.

Introduction

Angiogenesis is essential for the supply of nutrients and oxygen to cancer cells and greatly contributes to tumor growth, invasion and metastasis.[1, 2] Rapid cancer cell proliferation creates hypoxic, glucose-deprived environments that activate the so called "angiogenic switch". In these conditions, tumor cells begin to secrete a variety of diffusible pro-angiogenic factors, including Vascular Endothelial Growth Factors (VEGFs), which play a crucial role in stimulating neovascularization. VEGF is a potent mitogen for endothelial cells that binds its high affinity tyrosine kinase receptors (VEGFRs), triggering various intracellular signals promoting survival, division and migration of endothelial cells. In response, several other growth factors are secreted in the proximity of the newly formed capillaries finally stimulating the proliferation of cancer cells.[3] While VEGFR2 (known as Flk-1/KDR) is considered a major player in angiogenesis,[4] VEGFR1 (also known as Fms-like tyrosine kinase-, FLT1) acts as a regulator of angiogenesis (decoy protein for VEGF-A, the main ligand of VEGFR2) and is upregulated in endothelial cells undergoing growth and remodeling.[5, 6] VEGFR1 stimulation promotes pathological angiogenesis and triggers activation of protumoral M2 macrophages, which induce tumor cell proliferation and metastasis.[7] Furthermore, FLT1 is expressed in different cancer cell lines and upon stimulation with VEGF family members, tumor progression and spreading are activated.[7]

The evidence that VEGFR1-related signaling pathway participates in the "angiogenic switch" in tumors paved the way to targeting this receptor in anticancer therapies.[8] Indeed, some anti-VEGFR1 antibodies or inhibitory peptides have been proposed to arrest tumor growth and metastasis spreading

in various cancer models.[8-10] Nevertheless, only anti-angiogenic therapies interfering with the VEGF pathway mediated by both VEGFR2 and VEGRF1 have become a relevant and widely accepted approach for the treatment of cancer. A number of preclinical/clinical studies has confirmed that the inhibition of angiogenesis causes an arrest of the tumor growth and formation of metastasis. The approval of several antiangiogenic drugs acting as i) VEGF decoy (bevacizumab and other anti-VEGF antibodies), ii) tyrosine KINASE INHIBITORS INACTIVATING ALL VEGFRS, AND III) "VASCULAR-disrupting AGENTS" HAS THUS FOLLOWED.[3, 11, 12] However, their clinical use has faced severe limitations such as direct and indirect acquired resistance of cancer cells through induction of escape mechanisms and impaired oxygenation level, respectively. Cancer cell invasion, toxicity in normal organs, high blood pressure and bleeding are other drawbacks to consider during an antiangiogenic treatment.[13-16]

The delivery of antiangiogenic molecules through nanoparticulate systems may be considered a valuable strategy to overcome some of their main therapeutic limitations and confine antiangiogenic effects at tumor level. However, the development of antiangiogenic nanoplatforms for cancer therapy has been reported in a limited number of studies[17-19] while the delivery of single anti-angiogenic molecules or their combination with chemotherapeutics has been mainly attempted to improve pharmacokinetics and avoid undesired effects in healthy organs.[20-23]

In the context of combination therapies for cancer, polymeric nanoparticles (NPs) with core-shell architectures offer the advantage of easy manipulation of their overall features (size, surface hydrophilicity/charge, release rate, biodegradability) through appropriate tailoring of the chemistry of polymer

building blocks.[24-27] Furthermore, NPs can be logically designed to incorporate multiple drugs with different physical-chemical properties in the core or in the shell and deliver them at different release rates, which can be crucial to attain desired synergic/additive effects.[28-31] NPs made of amphiphilic block copolymers of poly(ethylene glycol) and poly(ε-caprolactone) (PEG-PCL) with different hydrophilic/lipophilic balance and architecture have been proposed to home poorly water-soluble chemotherapeutics to solid tumors due to their stability, sustained release features and degradability.[27, 32, 33] Furthermore, surface functionalization of PEG-PCL NPs with specific ligands, thus providing multifunctional NPs, has been proposed as a strategy to target drug cargo to specific cancer cells populations.[32]

Herein, we propose a novel approach to impart antiangiogenic properties to PEG-PCL NPs and provide a proof of concept of their therapeutic potential in delivering the poorly water-soluble chemotherapeutic docetaxel (DTX) in triple negative breast cancer cells. NPs with a hydrophobic core of PCL accommodating DTX and a hydrophilic shell of PEG exposing an anti-angiogenic short peptide sequence have been constructed..The peptide GNQWFI (aFLT1), selectively binding VEGFR1 isoform in vitro and inhibiting tumor growth and metastasis in a mice xenograft of VEGF-secreting cancer cells,[9] was covalently linked through click chemistry to the PEG -OH end to give an aFLT1-PEG-PCL copolymer. NPs were prepared from a mixture of PEG-PCL, with PEG molecular weight of 1000 Da, and aFLT1-PEG-PCL with PEG molecular weight of 1500 Da to promote aFLT1 exposition on NPs surface at appropriate ratios. NPs <100 nm entrapping DTX were obtained by nanoprecipitation. After an in-depth characterization aimed to assess shell properties, NPs were tested

in human umbilical vein endothelial (HUVEC) and breast cancer cell (MDA-MB-231) models as well as in chicken embryo chorioallantoic membranes (CAMs) xenografted with MDA-MB-231 cells to investigate the impact of DTX delivery though anti-angiogenic NPs on its anticancer activity.

Materials and Methods

Chemicals and reagents

Poly(ethyleneglycol) with Mn 1.5 kDa (PEG1.5k, Sigma-Aldrich, Milan, Italy) and monomethoxy-poly(ethyleneglycol) with Mn 1.0 kDa (mPEG1k, Nanocs Inc., USA) were dehydrated by azeotropic distillation with dry toluene in a Dean-Stark trap. ε-caprolactone (CL, Sigma-Aldrich, Italy) was distilled at reduced pressure over CaH_2. Trifluoroethanol (TFE) was purified as described in Purification of Laboratory Chemicals Armarego. Cu wires (Carlo Erba, Italy) were treated with H_2SO_4 for 10 min, washed twice with distilled water, methanol, and dried under reduced pressure at 60 °C for 30 min.

Docetaxel (DTX, MW= 807.88) was purchased from LC laboratories (USA). Triisoproylsilane (TIS), N-methylmorpholine (NMM), N,N dimethylformamide (DMF), sodium chloride, potassium phosphate dibasic and potassium phosphate monobasic, sodium azide, Rhodamine B isothiocyanate (Rhod), potassium chloride, sodium phosphate dibasic, sucrose, glucose, threalose, P188, mannitol, sorbitol, human serum albumin (HSA), human plasma and (2-Hydroxypropyl)-β-cyclodextrin (HPβCD, DS 0.6), were used as received (Sigma-Aldrich, Italy). Dialysis membranes (MWCO 3500, regenerated cellulose) were used as received (Spectrapor, Italy).

Peptide synthesis

Peptides aFLT1 (GNQWFI-NH_2), Pra-Ahx-aFLT1 (Pra-Ahx-GNQWFI), Reverse aFLT1 (IFWQNG-NH_2), Reverse Pra-Ahx-aFLT1 (Pra-Ahx-IFWQNG) (Pra: propargyl glycine, Ahx: amino hexanoic acid) were obtained by solid phase synthesis following standard protocols[34] on the Rink amide MBHA resin (0.54 mmol g^{-1}).

Peptides were cleaved off the resin and deprotected by treatment of the resin with a solution of TFA/TIS/H2O 95/2.5/2.5 v/v/v, 90 min. TFA was concentrated and peptides were precipitated in cold ethylic ether. Analysis of the peptides was performed by LC-MS ESI-TOF on a Agilent Technologies 6230 ESI-TOF instrument using a Phenomenex Jupiter 3 C18 (150 x 2.0 mm) column with a flow rate of 0.2 mL min-1. Analysis of the crudes was performed by LC-MS using a gradient of acetonitrile (0.1% TFA) in water (0.1% TFA) from 5 to 70% in 15 min. Peptides were purified by RP-HPLC ON A PHENOMENEX JUPITER 10µ PROTEO 90 Å (250×10 MM) USING A gradient of acetonitrile (0.1% TFA) in water (0.1% TFA) from 5 to 70% in 20 min.

The peptide derivatized with rhodamine, named Rhod-Ahx-aFLT1 (Rhod-Ahx-GNQWFI) was obtained as follows. To the resin bound a peptide, the Fmoc-Ahx-OH linker was coupled and Fmoc deprotected following standard procedures for peptide synthesis. Rhod (10 Eq) was dissolved in DMF, NMM (14 Eq) was added; the solution was reacted with the peptide 3 h at r.t. and another coupling was performed overnight. Peptides were cleaved off the resin and deprotected by treatment of the resin with a solution of TFA/TIS/H2O 95/2.5/2.5 v/v/v, 90 min. TFA was concentrated and peptides were precipitated in cold ethylic ether. Analysis of the crudes was performed by LC-MS ESI-TOF using a gradient of acetonitrile (0.1% TFA) in water (0.1% TFA) from 5 to 80% in 15 min. Peptides were purified by RP-HPLC using a gradient of acetonitrile (0.1% TFA) in water (0.1% TFA) from 5 to 80% in 20 min.

aFLT1 sequence: GNQWFI-NH_2, Calculated mass (Da): 762.83; found: [M+2H]2+= 382.68.

Reverse aFLT1 sequence: IFWQNG-NH_2. Calculated mass (Da): 762.83; found: $[M+2H]^{2+}$= 382.27.

Pra-Ahx-aFLT1 sequence: Pra-Ahx-GNQWFI. Calculated mass (Da): 970.43; $[M+2H]^{2+}$= 486.21; found: 970.25; $[M+2H]^{2+}$= 486.09;

Rhod-Ahx-aFLT1 (Rhod-Ahx-GNQWFI) Calculated mass (Da):1374.80; found: [M+2H]2+ 688.33

Reverse Rhod-Ahx-aFLT1 (Rhod-Ahx- IFWQNG) Calculated mass (Da):1374.80; found: [M+2H]2+ 688.33

Copolymer synthesis

Synthesis of mPEG-PCL diblock copolymer. Linear mPEG-PCL diblock copolymer was prepared by ring-opening polymerization (ROP) of CL at 120 °C for 24 h using mPEG1k as initiator and Sn(Oct)2 as catalyst (20% by mol), as previously reported.26 CL/initiator molar ratio = 36. 1H NMR (CDCl3, δ in ppm), PCL block: 1.29–1.78 (m), 2.19–2.43 (t) 3.20 (m); 3.92–4.21 (t), 4.31(t); PEG block: 4.10 (t), 3.64 (s), 3.38, (t); Mn of PCL block evaluated by NMR: 4.4 kDa.

Synthesis of mPEG-PCL-Rhod diblock copolymer. mPEG-PCL (500 mg) was dissolved in 10 mL of dry chloroform, then DCC (41.6 mg, 0.2 mmol), DMAP (24.4 mg, 0.2 mmol) and Rhod (95.8 mg, 0.2 mmol) were added and the solution was left under stirring at room temperature overnight. The polymer was precipitated in diethylether and repeatedly washed (yield 92%). Washing solvent was analyzed by UV-vis absorption to exclude residual free Rhod (λ=360 nm). The amount of Rhod on the copolymer was quantified by UV-vis spectroscopy on DMSO solutions, using Rhod standard solutions as calibration curve (Rhod: 5%, functionalization degree: 74%).

Synthesis of aFLT1-copolymer conjugate (aFLT1-PEG-PCL). Azido-PEG-PCL copolymer (N3-PEG-PCL) was prepared starting from PEG1.5k according to a procedure reported elsewhere.26 FTIR diagnostic band: 2097 cm-1 (azide); 1H NMR (CDCl3, δ in ppm): 3.6 (2H, t), 3.5 (127H, s, PEG backbone), 3.4 (2H, t), 1.29–1.78 (139H, m); 2.19–2.43 (82H, m), 3.92–4.21(82H, t) 4.31,(2H, t); Mn of PCL block evaluated by NMR = 4.6 kDa.

In a flask equipped with N2 inlet, N3-PEG-PCL (0.02 mmol, 144 mg) and Pra-Ahx-aFLT1 (0.031 mmol, 30 mg) were dissolved in 2 mL of TFE/DMF (30/70 v/v) under nitrogen stream. Cu wires (100 mg) were added and the reaction was carried out at 40° C for 48 h under mechanical stirring. The reaction mixture was protected from light by aluminum foil. After removal of Cu wires and evaporation of solvent, the product was dissolved in THF and the solution was filtered with a screw filter 0.22 μm PTFE. The insoluble fraction, consisting of unreacted aFLT1, was weighed (7.56 mg, corresponding to 25% of the total peptide; conjugation degree: 75%). The THF solution containing aFLT1-PEG-PCL conjugate was finally purified by passing over neutral alumina to remove copper. The conjugate was recovered by THF evaporation at reduced pressure (yield 83%). FTIR diagnostic bands (cm-1): 2097 (N3 stretching), 1736 (C=O stretching), 1650 (amide I band), 1540 (amide II band).

NPs preparation

aFLT1-decorated NPs were prepared from a mixture of mPEG-PCL with aFLT1-PEG-PCL (mPEG-PCL/aFLT1-PEG-PCL weight ratio 9:1) (DBL_{aFLT1}) whereas NPs without aFLT1 (DBL) were prepared from mPEG-PCL. NPs were formed by solvent diffusion of an organic phase (10 mg of copolymer mixture in 1 mL of acetone) added dropwise in water (2 mL) under magnetic stirring (500 rpm). After solvent

evaporation, NPs were filtered through 0.45 μm Phenex® filters (Phenomenex, USA). NPs were freeze-dried after the addition of HPβCD as cryoprotectant (polymer: HPβCD 1:10 wt. ratio) and subsequent 1:10 dilution in water. NPs loaded with DTX were prepared according to the procedure reported above by co-dissolving DTX with the copolymer(s) (10% w/w) in the organic phase. To evaluate cellular uptake, fluorescent NPs were prepared according to the procedure reported above by using a mixture of mPEG-PCL, mPEG-PCL-Rhod and aFLT1-PEG-PCL (weight ratio 8:1:1).

NPs characterization

Hydrodynamic diameter (DH), polydispersity index (PI) and zeta potential (ξ) of NPs were determined on a Zetasizer Nano Z (Malvern Instruments Ltd). Results are reported as mean DH of three separate measurements of three different batches (n = 9) ± standard deviation (SD). Yield of NP production process was evaluated on an aliquot of NP dispersion by weighting the solid residue after freeze-drying. Results are expressed as the ratio of the actual NP weight to the theoretical polymer weight × 100.

Fixed aqueous layer thickness (FALT) of NPs was measured by monitoring the influence of ionic strength on zeta potential (ξ). Different amounts of NaCl stock solutions were added to NPs dispersed in water (500 μg mL) and ξ of the samples measured. The plot of ln ξ against 3.33[NaCl]0.5 gives a straight line where the slope represents the thickness of the shell in nm.[35]

The exposition of aFLT1 on the surface of DTX-DBL$_{aFLT1}$ was evaluated using LavaPep™ Peptide and Protein Quantification Kit (Gel Company). A serial dilution of aFLT1 free in water was prepared (2-200 μg mL^{-1}) and the samples were incubated with working solution in the dark for 60 min at r.t. Using

fluorescence microlitre plate reader (Glomax Explorer, Promega, Italy), the fluorescence was evaluated with the 540±10 nm excitation and 630±10 nm emission filters. The same protocol was used to quantify the amount of aFLT1 on NP surface directly using NP dispersion. The results are expressed as % exposition ± SD of three experiments.

In order to evaluate the interaction of NPs with HSA, DBL and DBL_{aFLT1} were placed in a HSA solution with different concentrations of HSA in water and then analyzed by fluorescence spectroscopy and size measurements. The fluorescence emission spectra of HSA (500 μM), in the absence and in the presence of NPs (5 mg mL-1) upon excitation at 278 nm, were collected in order to explore the fluorescence behavior of NPs and the possible static quenching effects by the massive aggregation of HSA on NPs (RF6000 spectrofluorimeter, Shimadzu, Japan). Similarly, 1.5 mg of NPs (in 500 μL of water) were diluted with a HSA solution (1-500 μM) or 250 μl of human plasma and incubated at 37 °C for different times. Hydrodynamic diameter (DH), polydispersity index (PI) and zeta potential (ξ) of NPs were determined on a Zetasizer Nano Z (Malvern Instruments Ltd).

DTX actual loading and release

DTX loading inside NPs was assessed by placing 1 mg of freeze-dried NPs (without cryoprotectant) in 500 μL of acetonitrile, adding 500 μL of water and filtering the samples through a 0.45 μM filter (Phenomenex, USA). DTX was analyzed by HPLC using a Shimadzu (Japan) apparatus equipped with a LC-10ADvp pump, a SIL-10ADvp autoinjector, a SPD-10Avp UV-Vis detector and a C-R6 integrator. The analysis was performed using a Juppiter 5 μM, C18 column (250 x 4.6 mm, Å) (Phenomenex, USA). The mobile phase was a 55:45 (v/v) mixture of

water with 0.1% TFA and acetonitrile pumped at a flow rate of 1 mL min−1. The UV detector was set at 227 nm. A calibration curve for DTX in ethanol was plotted in the concentration range of 2–200 μg mL−1.

The release of DTX was determined on 0.5 mg NPs dispersed in 0.5 mL of 10 mM phosphate buffer containing NaCl (137 mM) and KCl (2.7 mM) at pH 7.4 (PBS) at 37°C in a dialysis bag immersed in an external phase (5 mL) of the same medium. At predetermined times, 1 mL aliquots of the sample were collected and then analyzed by HPLC to evaluate the actual loading of DTX in NPs. The results are expressed as % release ± SD of three experiments.

Cell lines

All cell lines were obtained from American Type Culture Collection (ATCC, Rockville, USA). HUVEC (human umbilical vein endothelial cells) were cultured in Medium-200 supplemented with antibiotics (100 U mL^{-1} Penicillin G and 100 μg mL-1 Streptomycin) and with the Low Serum Supplement Kit (Life Technologies) having a final fetal bovine serum (FBS) concentration of 2%. MDA-MB-231 cells were grown in DMEM supplemented with 10% FBS and antibiotics. All cell lines were maintained at 37 ◦C in a humidified atmosphere containing 5% CO_2. All the in vitro studies were performed with NP dispersions immediately after preparation.

Tube formation assay

Geltrex® Matrix (Geltrex® LDEV-Free Reduced Growth Factor Basement Membrane Matrix, Life Technologies) was thawed at 4 °C overnight. Each well of pre-chilled 24-well/plates was coated with 100 μL of matrix, incubated and solidified at 37 °C for at least 30 min. Meanwhile, HUVEC (cultured for

maximum 4 passages from thawing) were harvested from flasks and seeded (4.8 x 104 cells/well) in M200 medium supplemented with LVES (Large Vessel Endothelial Supplement, Gibco) for 18 h. During cell seeding, in each well, free PEPTIDES (100 μM) OR NPS (50 μG ML-1) OR DTX (5 μG ML-1) loaded or not in NPs were added. Wells containing untreated HUVEC were used as positive controls of tube forming cells while HUVEC incubated with 0.01% DMSO were employed as negative control. After 18 h of incubation, the cells were washed with PBS WITH CA2+ AND MG2+, INCUBATED AT 37 °C WITH CALCEIN AM 2 μM (MOLECULAR Probes) for 15 min, washed again and maintained in M200 medium until the end of the image acquisition. Tube formation was analysed using an inverted fluorescence microscope (DMI4000, Leica) at 5x or 10x magnification. Image analysis was performed from randomly selected fields using a dedicated plug-in (Angiogenesis Analyzer) for Image J and the percentage of inhibition in treated cells vs control cells was reported for the formed numbers of junctions, master segments and meshes.

Cytotoxicity

The viability of HUVEC and MDA-MB-231 cells incubated with increasing concentrations of free DTX dissolved in standard solution (DMSO) or loaded in DBL or DBL_{aFLT1} NPs was measured with the MTS assay (CellTiter 96® AQueous One Solution Cell Proliferation Assay, Promega Co., Madison, USA). The viability was measured also in cells incubated with empty DBL or DBL_{aFLT1} NPs to check the safety of the delivery system. For MTS assay, cells (8×10^3 MDA-MB-231 or 7×10^3 HUVEC) were seeded in 96-well plates and, after 24 h of growth, incubated with the various formulations diluted in cell medium added with 10% FBS. Cell viability was measured after 48 and 72 h of incubation. For the MTS ASSAY THE CULTURE MEDIUM WAS REPLACED WITH 100 μL OF SERUM-free medium

and 20 µL of the CellTiter 96® reagent and the wells were incubated for 1 h at 37 °C. The absorbance at 492 nm was measured using a Multiskan Go (Thermo Fischer Scientific, Waltham, USA) plate reader and the viability of treated cells was expressed as percentage of the absorbance of control cells that was taken as 100% viability. The Primer software for biostatistics (McGraw-Hill, Columbus, USA) was used for statistical analysis of the data. The data are expressed as means ± standard deviations (SD) for at least 3 independent experiments. The difference between groups was evaluated with the Student's t-test and was considered significant for $p < 0.05$.

Chicken embryo chorioallantoic membrane (CAM) assay

The CAM model was used to evaluate anti-angiogenic effects, tumor growth delay, metastasis inhibition and toxicity induced by DTX-loaded DBL and DBL_{aFLT1} NPs. Fertilized chicken eggs were incubated at 37.5 °C with 50% relative humidity for 9 days. At this time (E9), the CAMs were dropped by drilling a small hole through the eggshell into the air sac and a 1 cm^2 window was cut in the eggshell above the CAM. Thereafter, MDA-MB-231 cells (90% confluence, passage 12), cultured as indicated above, were re-suspended in graft medium and inoculated (10^6 cells) onto the CAM of each egg. Twenty-one eggs were used for each condition and randomized into 5 groups. The day after induction (E10), the tumors began to be detectable and the treatment started once a day for a total of 5 consecutive days (days E10- E14, see scheme 1). HPβCD-NPs freeze-dried formulations (without or with DTX) were dispersed in PBS while free DTX was solubilized in a 1% DMSO in PBS, achieving a final DTX concentration of 1 µM (100 µl of tested samples were employed). The daily doses of DTX and NPs were, respectively, 0.083 and 0.83 µg. Negative control samples were inoculated with 100 µL of PBS.

For evaluating the anti-angiogenic effects, images (8-12 upper CAMs per group) of tumors with associated vessels were taken at E15. On these images, the number of vessels arriving on tumors was counted (3 different counts for each sample). A one-way ANOVA analysis with post-tests was applied on data. For measuring the tumor size, the upper portion of the CAM with tumors was removed at E16, washed in PBS and immediately fixed in paraformaldehyde for 48 h. The normal CAM tissue around the tumors was carefully removed and the tumors were weighed. A one-way ANOVA analysis with post-tests has been done on these data. At E16, a 1 cm2 portion of the lower CAM, distant from the site of tumor cells implantation, was also collected to evaluate the number of metastatic cells (invasion analysis). Genomic DNA was extracted from the CAM, and analyzed by qPCR with specific primers for the human specific Alu sequences.[36] Statistical analysis was directly performed on data from the Bio-Rad CFX Maestro software.

The toxicity of the different treatments on embryo viability was monitored at E16 by counting the dead embryos as well as observing eventual visible macroscopic abnormalities.

Results and discussion

Synthesis and characterization of aFLT1-PEG-PCL conjugate

AntiFLT1 peptides were obtained in highly pure form in two different variants: the free peptide (GNQWFI) and the alkyne derivatized peptide (Pra-Ahx-GNQWFI). The propargyl glycine (Pra), needed for the click reaction with the azide-functionalized polymer was separated from the peptide by an amino hexanoic acid linker so that the alkyne was less sterically hindered and therefore available for the click reaction. As a control, we also prepared GNQWFI conjugated with Rhod and a peptide with reverse sequence (IFWQNG).

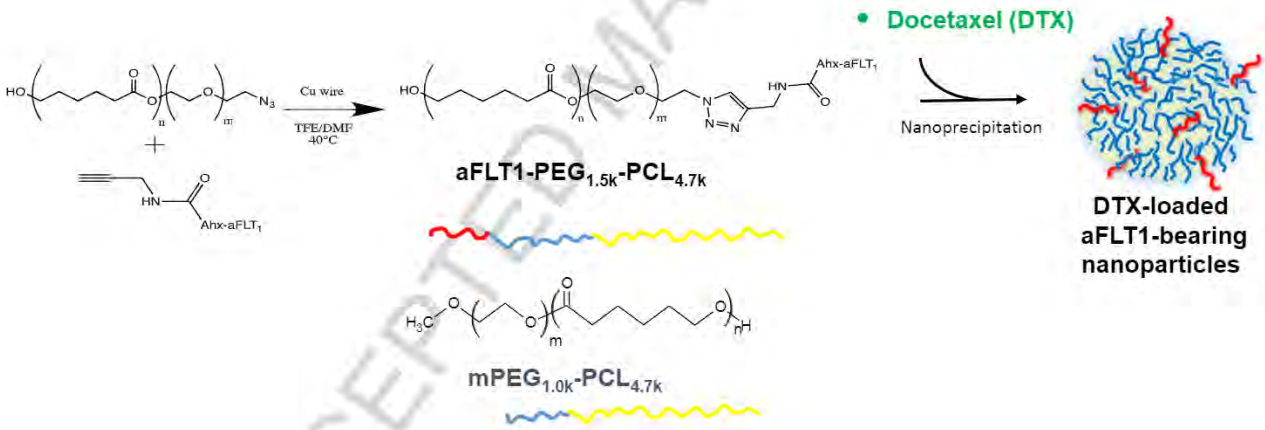

Figure 1. Synthesis of aFLT1-PEG-PCL and structure of antiangiogenic NPs.

Copper(I)-catalyzed alkyne-azide 1,3-DIPOLAR CYCLOADDITION (CUAAC) "CLICK" reaction was used to conjugate the peptide to N_3-PEG-PCL copolymer. This reaction has been widely used for conjugation of peptides, drugs and other biological molecules to synthetic azide/alkyne-functionalized polymers, and particularly to PEG.[37] The reaction can be performed by using different Copper sources (Cu(I) salts, Cu(II) salts, solid Cu(0)). For peptide conjugation,

the catalyst is better prepared in situ by reduction of Cu(II) salts, which are often purer than Cu(I) salts, in presence of a reducing agent. The Cu(SO4)/ascorbate system is often reported for peptides conjugation in aqueous medium. In the case of water insoluble copolymers such as PEG-PCL, Cu(0) in form of wires, turnings, powder or colloidal particles has been used as source of Cu(I) catalyst, with or without addition of Cu(II) salts, base or ligand (Figure 1).[38]

For antiFLT1 coupling, the reaction was carried out in a TFE/DMF mixture to promote unfolding of the peptide and to promote the exposition of alkyne group for click reaction. As a matter of fact, preliminary tests confirmed that addition of TFE increases the final conjugation ratio. At the end of the reaction, after solvent and Cu wires removal, the product was dissolved in THF and separated from the unreacted peptide (insoluble) by filtration. The formation of the conjugate was confirmed by FTIR spectroscopy, which showed a significant decrease of the azide band at 2097 cm^{-1} in comparison to that of the initial copolymer, and the appearance of the characteristic amide I and amide II bands, attributed to peptide bonds (Figure S1). The substitution degree was estimated from FTIR spectra comparing the ratio between the absorbance intensities of azide peak and PCL carbonyl peak (1736 cm^{-1}) of peptide-copolymer conjugate to corresponding ratio of N_3-PEG-PCL copolymer. The conjugation efficiency was ~70% in good agreement with the value calculated through gravimetric measurement of unreacted peptide (~75%).

Properties of aFLT1-decorated NPs

Anti-angiogenic NPs were prepared from a mixture of mPEG-PCL with aFLT1-PEG-PCL copolymers (DBL_{aFLT1}) and their properties compared to those of NPs

prepared from mPEG-PCL diblock copolymer (DBL). Solvent diffusion method, currently indicated as nanoprecipitation, was selected since it is suggested as valid option to produce NPs in an industrial setting and thus to increase the scale of NP production. Colloidal properties of NPs in terms of size, polydispersity index (PI), zeta potential (ζ) and entrapment efficiency of DTX are reported in Table 1.

Table 1. Overall properties of unloaded and DTX-loaded NPs.

NPs formulation	Size (nm ± SD[a])	PI	ζ (mV ± SD[a])	Yield (%± SD[a])	DTX Actual loading (mg DTX/100 mg NPs)	DTX Entrapment Eff. (%)	aFLT1 exposition (%± SD[a])
DBL	78±2	0.1	-12±0.1	68±4	-	-	-
DBL_{aFLT1}	78±5	0.1	-10±2.0	60±2	-	-	19±1.9
DTX-DBL	92±7	0.2	-9.8±0.3	72±6	8.8±0.9	96±2.3	-
$DTX\text{-}DBL_{aFLT1}$	78±4	0.1	-9.4±1.5	75±3	8.5±0.6	95±1.7	20±1.3

We obtained NPs formulations in high yield without the help of any surfactant with a size below 100 nm and low PI (< 0.2). The ξ was slightly negative as commonly found for PEGylated NPs and unaffected by the incorporation of the aFLT1-modified copolymer. To guarantee long term stability of the formulations, we attempted to freeze-dry NPs in the presence of HPβCD as cryoprotectant, as already reported.[39] However, due to the limited shielding of short PEG chain length on particle-particle interactions, previous conditions were not successful and detailed freeze-drying studies were needed. Different cryoprotectants at different weight ratio with the NPs and different NPs concentration were tested (Table S1). The screening allowed identification of the best freeze-drying conditions when using HPβCD in the ratio 1:10 to NPs and successive 1:10 NP sample dilution, since on these

conditions no significant diameter and PI changes were observed after NP re-suspension. Furthermore, in this work the covalent linkage between the diblock copolymer and the anti-FLT1 hexapeptide does not modify the colloidal properties of NPs after redispersion. Preliminary stability studies on freeze-dried powders stored at 4 °C (Table S2) demonstrated that key parameters of NPs were unchanged after one month.

The amount of aFLT1 exposed on NPs surface was evaluated through a fluorimetric assay. Independently on DTX encapsulation, the amount of aFLT1 on the surface was much lower than expected (~20%), suggesting that, in the conditions adopted to produce NPs, the peptide is partly located inside the NP core or is in the surface layer but buried in the PEG chains. Nevertheless, the thickness of the external hydrophilic shell of NPs, as evaluated by FALT (Figure 2A), was 4.9 nm for DBL_{aFLT1} and much lower for DBL (2.5 nm) in line with previously reported results.[40] These data suggest that a different arrangement of PEG chains on NP surface due to the presence of the peptide is achieved.

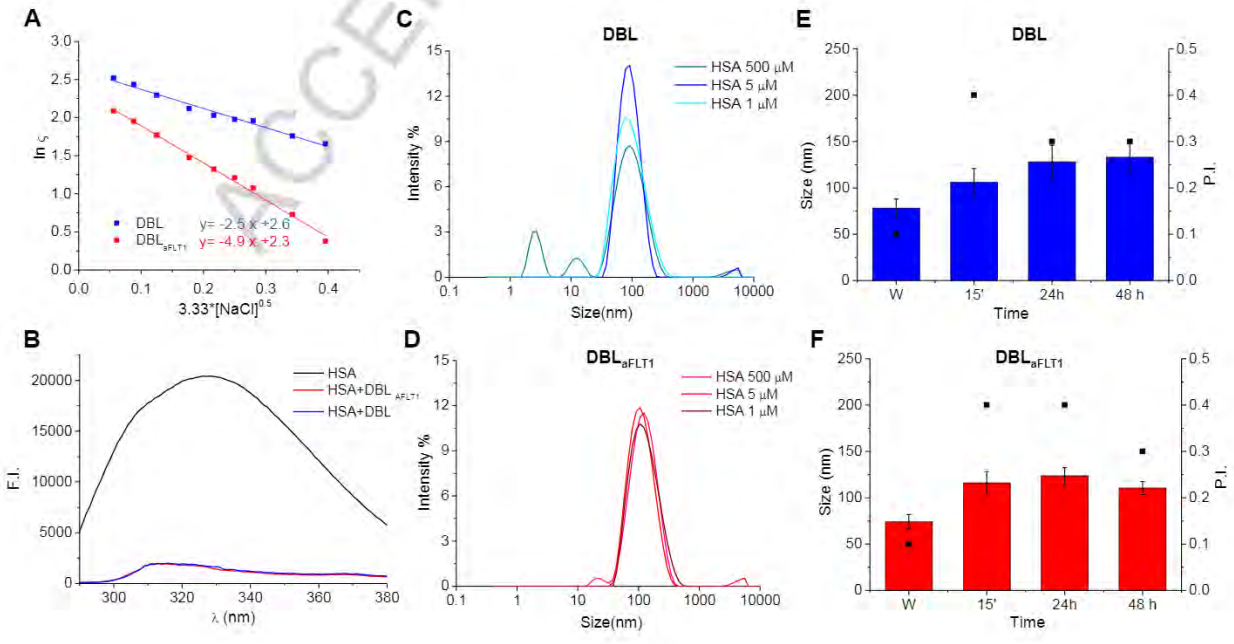

Figure 2. Properties of NPs. A) FALT measurements: the slope of the straight line represents the thickness of the outer hydrophilic shell in nm; B) Fluorescence emission spectra of 500 μM HSA in the absence and in the presence of 5 mg mL-1 NPs; C) and D) Size distribution of NPs in the presence of increasing concentration of HSA; E) and F) Mean size (bar) and PI (square) of NPs after incubation for different times in human whole plasma at 37 °C.

Interaction of aFLT1-decorated NPs with protein-rich media

It is well known that the conformation of PEG on NP surface can drive the interactions with serum proteins profoundly affecting NP biodistribution and interaction with different cell populations.[41, 42] The impact of aFLT1 on the interaction of NPs with human serum albumin (HSA), the most abundant plasma protein, as well as whole human plasma was thus investigated. To this purpose, the fluorescence emission spectra of HSA in the absence and presence of NPs were collected upon excitation at 278 nm, which reflect the contribution of the tyrosine (λem ca 310 nm) and tryptophan (λem ca 340 nm) fluorogenic centers (Figure 2B). The strong HSA emission was quenched by more than one order of magnitude upon addition of both kind of NPs formulations, thus suggesting a massive interaction between NPs and the protein. The formation of a HSA corona on NPs was confirmed by the changes of the size distribution curves of NPs at increasing HSA concentration (Figure 2C and 2D).

However, through this experiment, we observed a different behavior between DBL and DBL_{aFLT1} NPs. In the case of DBL, ADDITION OF HSA UP TO 5 μM DID NOT change greatly the shape of the size curves, while at physiologically

relevant HSA concentration (500 μM) NP size intensity was reduced. In particular, the appearance of the peaks at 3 and 11 nm corresponding to free HSA monomers/tetramers/hexamers, indicates that in these conditions, the surface of NPs is fully occupied by HSA. In contrast, size curve distribution of DBL_{aFLT1} NPs did not change significantly in the presence of HSA, thus suggesting the formation of a soft protein corona on NP surface without inducing their aggregation, probably due to different thickness of the hydrophilic shell and organization of hydrophilic PEG/aFLT1 chains as previously suggested.

To reproduce the biological conditions encountered by NPs during i.v. injection, the stability of NPs in human plasma until 48 h of incubation was evaluated. As shown in Figure 2E and 2F, both DBL and DBL_{aFLT1} NPs showed a slight increase of size (which was however below 150 nm) and a slight increase of PI, thus demonstrating adequate stability in simulated biological conditions. These results are in line with further stability studies carried out by dispersing NPs in different media, including PBS at pH 7.4 and DMEM with 10% FBS (Figure S2).

Effect of aFLT1-decorated NPs on HUVEC tube formation

The capability of the synthesized aFLT1 peptide to bind VEGFR1 was first assessed in HUVEC cells, which are known to overexpress this receptor.[43] As confirmed in Figure S3A, in the adopted experimental conditions, VEGFR1 was highly expressed by HUVEC as documented by specific antibody recognition and flow cytometry analyses. A significantly higher interaction of the Rhod-

conjugated aFLT1 peptide (Rhod-Ahx- aFLT1) compared to the reverse peptide (Rhod-Ahx- reverse aFLT1) was observed in HUVEC cells (Figure S3B). The results of competition experiments carried out using the VEGFR1 and VEGFR2 specific ligand VEGF165, showed a significant ($p<0.005$, t test) inhibition of aFLT1 interaction after co-incubation of HUVEC with 50 ng mL-1 VEGF165, indicating that aFLT1 peptide and VEGF165 competed for the binding to VEGFR1. On the contrary, no significant inhibition in peptide interaction was measured for the peptide with reverse sequence, confirming its inability to interact with VEGFR1 and to affect VEGFR ligands interaction. Overall, our results are in agreement with those reported by Bae and coworkers,16 who verified the VEGFR1-specific character of the aFLT1 peptide with purified recombinant proteins and measured a 60% inhibition of VEGF165 binding to VEGFR1 in the presence of aFLT1 peptide in HUVEC. Furthermore, aFLT1-decorated NPs were internalized by HUVEC as shown by confocal microscopy on rhodamine-labeled DBL_{aFLT1} (Fig S3D).

To assess whether the covalent binding of aFLT1 on NPs surface could alter its antiangiogenic activity, we performed an in vitro endothelial tube formation assay in HUVEC. Figure 3A shows representative images of the tubes formed in the presence of different antiangiogenic agents and Figure 3B summarizes the results obtained from the analysis of the images with the ImageJ dedicated plugin (Angiogenesis Analyzer).

The number of junctions, master segments and meshes were reported in Figure 3B as the most significant parameters. Surprisingly, the aFLT1 peptide conjugated to NPs (DBL_{aFLT1} at 50 μg mL-1) demonstrated significantly higher anti-angiogenic activity (at least two times) than the free peptide in reducing all the three parameters considered for evaluating the antiangiogenic

activity (in both cases aFLT1 was 100 μM). As expected, no effects on tube formation were detected for the free reverse peptide. Similarly, DBL caused only a slight (~ 10%) reduction of the number of junctions but did not affect the number of master segments and meshes of the endothelial tubes. It is worth noting that NPs were not cytotoxic for HUVEC until 72 h at the tested concentration (50 μg mL-1) (Figure S4). Thus, it appears clear that the anti-angiogenic activity of the DBL_{aFLT1} can be attributed exclusively to the presence of aFLT1 peptide on NP surface, even though only 20% of the peptide was exposed.

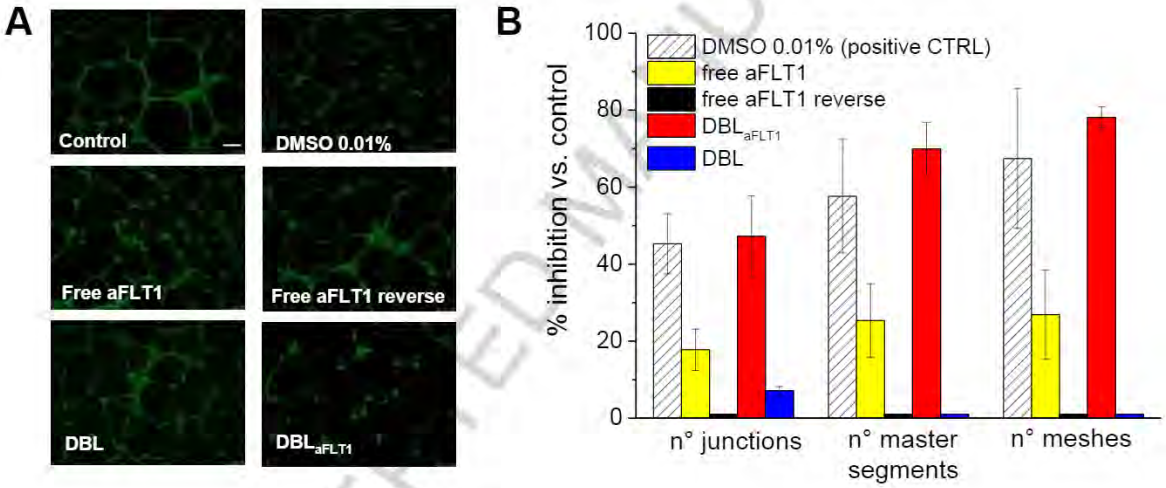

Figure 3. In vitro endothelial tube formation assay in HUVEC. A) Representative fluorescence images of tubes and B) summary of results on percent inhibition of tube formation with the different treatments. Inhibition caused by cell incubation for 18 h with 50 μg mL^{-1} of DBL or DBL_{aFLT1} or with the corresponding dose of free aFLT1 (100 μM) or its reverse sequence peptide. Cell incubation with 0.01% DMSO was used as positive inhibitor of tube formation. Scale bars: 250 μm.

Properties of DTX-loaded NPs and cytotoxicity on MDA-MB-231 and HUVEC

DTX was loaded in the core of NPs after dissolution in the polymer mixture. Some properties of drug-loaded NPs are reported in Table 1. The size of DTX-DBL was slightly larger as compared to the other formulations while ζ remained negative. The amount of aFLT1 on NPs surface was unchanged upon drug encapsulation and NPs were stable in both water and PBS (Figure 4A). The release of DTX from NPs was evaluated in 10 mM PBS, pH 7.4 at 37 °C through the dialysis method. DTX entrapped at 10% theoretical loading was almost completely associated to NPs, without any significant difference for copolymer material employed (Table 1).

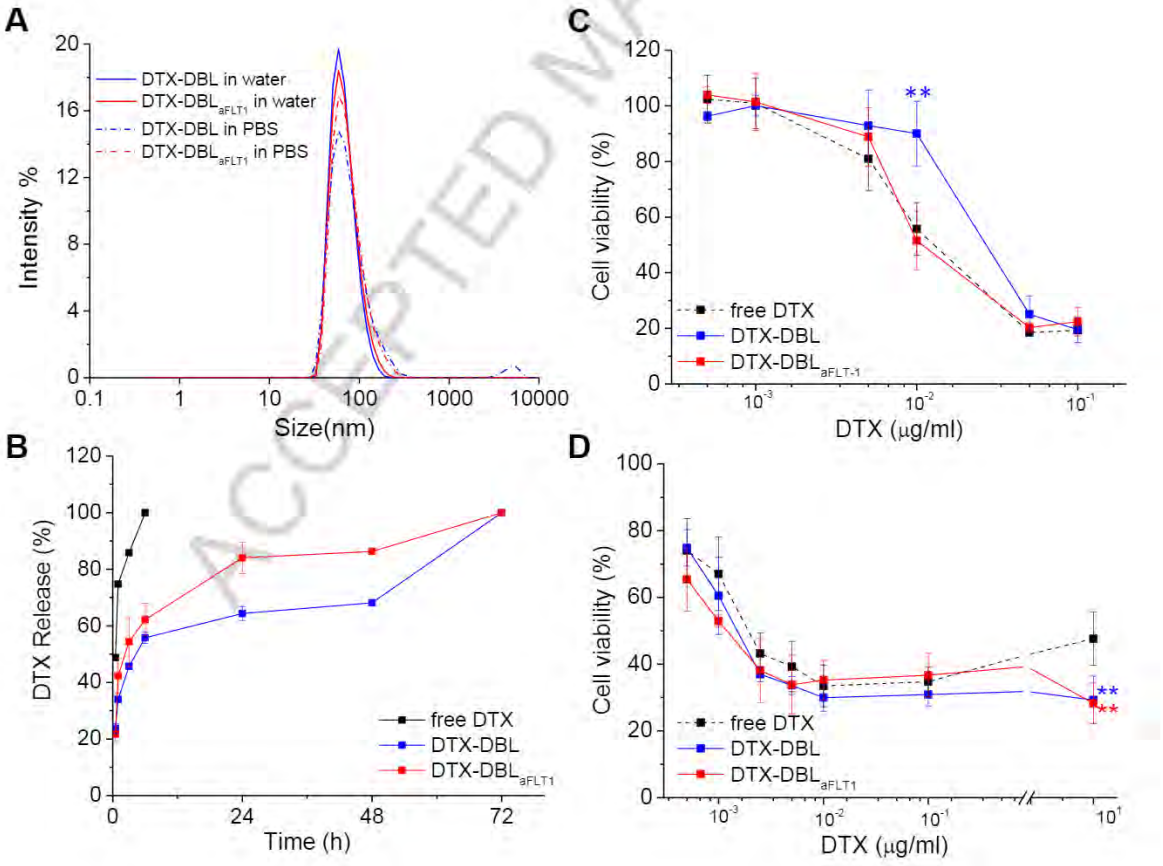

Figure 4. Properties and cytotoxicity of DTX-loaded NPs. A) Size distribution of DTX-loaded NPs in water and PBS pH 7.4; B) DTX release from NPs in PBS 10 mM pH 7.4, at 37 °C evaluated by dialysis method. Results are the means ± SD of three measurements obtained on three different NPs batches. Cytotoxicity in C) MDA-MB-231 cells and D) HUVEC of DTX delivered in DMSO or loaded in DBL or DBL_{aFLT1}. Cell viability was measured with the MTS assay after 72 h of cell incubation. Data are mean values ± SD of at least three independent experiments carried out in triplicate. *p value<0.005, vs. free DTX; **p value<0.001, vs. free DTX (STUDENT'S *t* test).

Due to its good compatibility with PCL phase, DTX is assumed to locate in NPs lipophilic core. As evident in Figure 4B, in both DTX-DBL and DTX-DBL_{aFLT1} NPs we observed a fast release of about 50% of the drug during the first 6 h followed by a slow release rate indicating that NPs are able to sustain drug release along time as compared to free drug (100% release in 6 h). The overall results are in line with our previous studies on DBL demonstrating that DTX was released slowly as typical for a sustained-release nanosystem.[39] Furthermore, the presence of aFLT1 on NP surface does not affect greatly the overall release rate of the hydrophobic drug entrapped in the internal core.

MTS assay was employed to measure viability reduction in triple negative MDA-MB-231 breast cancer cells (Figure 4C) and HUVEC (Figure 4D) incubated for up to 72 h with free DTX or loaded in DBL or DBL_{aFLT1}. The viability curves in MDA-MB-231 cancer cells showed a clear dose-dependent cell mortality, that was more than 80% after 72 h of treatment at the highest DTX dose tested (0.1 μg mL-1) for all the formulations. In some cases (e.g. 0.01 μg mL-1 DTX), DTX-DBL were significantly less cytotoxic than free DTX or DTX-DBL_{aFLT1} NPs also

after 48 h (Figure S5). Since MDA-MB-231 do not express full-length Flt1 or soluble FLT1 it is plausible that both the slower release of DTX from DBL and the different amount of NPs uptaken play a role. Some contributions of the delivery system in determining cell toxicity was excluded by measuring the viability of MDA-MB-231cells incubated with empty DBL or DBL_{aFLT1} up to 100 μg mL-1 NPs, corresponding to the highest DTX tested dose (Figure S4). Overall, the results show that DTX-DBL and DTX-DBL_{aFLT1} NPs exert similar cytotoxic activity toward MDA-MB-231 cells and, importantly, not lower than that of free DTX.

The shape of the viability curves in HUVEC was completely different and comparable cytotoxicity after 72 h of incubation for all the tested concentrations was observed, with the exclusion of the highest concentration (e.g. 10 μg mL-1) at which DTX-loaded NPs were significantly more effective with respect to the free chemotherapeutic. This behavior was observed also after 48 h incubation (Figure S5A). Notably, the viability curves of HUVEC showed a clear plateau around 50% and 40% viability after 48 and 72 h of incubation, respectively, for DTX doses ranging from 0.005 to 10 μg mL-1, indicating that a fraction of these cells are not sensitive to DTX.

It is well known that DTX exerts its antineoplastic activity by inhibition of microtubule depolymerization in different cancer cell lines blocking proliferation. Obviously, these effects are not limited to transformed cells and endothelial disfunction and apoptosis has been reported for DTX at nM concentration in HUVEC and related to both an analogous mechanism[44] or upregulation of oxidative stress.[45] In the attempt to explore the impact of DTX or DTX-loaded NPs at a concentration (5 μg mL-1), cytotoxic for MDA-

MB231, on antiangiogenic activity, the endothelial tube formation assay was performed. In the experimental conditions adopted, free DTX or NPs formulations showed no cytotoxicity in HUVEC after 24 h (Fig 5A). DTX-DBL$_{aFLT1}$ gave the highest antiangiogenic effect and was able to completely abolish mesh formation (Fig 5B). Free DTX demonstrated an antiangiogenic activity comparable or slightly increased with respect to that of free aFLT1 peptide (Figure 3 A and B), while its encapsulation in DBL resulted in a significant reduction of activity ($p<0.001$, t test for all the three considered parameters).

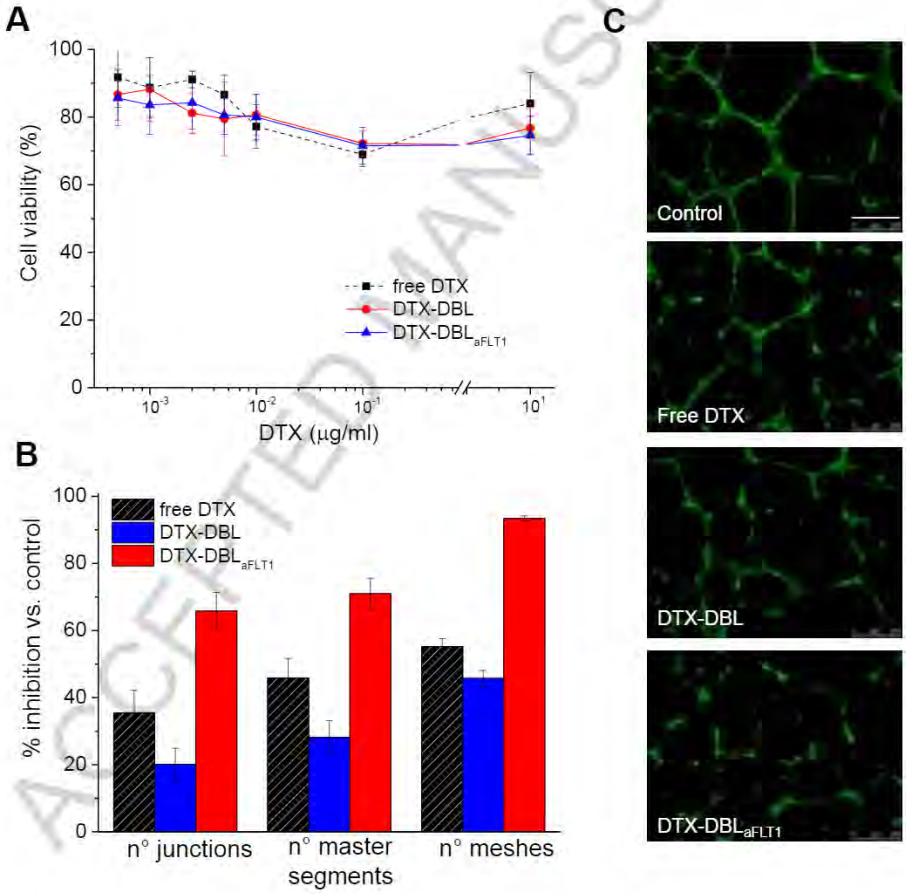

Figure 5. Cytotoxicity and endothelial tube formation assay in HUVEC cells of DTX and DTX-loaded NPs. A) Cytotoxicity of DTX delivered in the standard solvent or loaded in DBL or DBL$_{aFLT1}$ NPs in HUVEC cells. Cell viability was measured with the MTS assay after 24 h of cell incubation. Data are mean values ± standard deviation of at least three independent experiments

carried out in triplicate. B) Summary of results on percent inhibition of tube formation with the different treatments and C) Representative fluorescence images of tubes. Inhibition caused by cell incubation for 18 h with 50 μg mL-1 of DBL or DBL_{aFLT1} or with the corresponding dose of free DTX (5 μg mL-1). Scale bars: 250 μm.

In any case, the inhibition of the number of junctions and meshes with DTX-DBL_{aFLT1} was significantly potentiated compared to unloaded DBL_{aFLT1} ($p<0.001$, t test), while the number of master segments was not ($p>0.05$, t test).

Overall, the results confirmed that NPs decorated with aFLT1 are more potent anti-angiogenic system with respect to the free peptide and the loading of NPs with the chemotherapeutic drug does not affect but potentiate the inhibition of formation of properly conformed tubes (e.g. no meshes formed at all with DTX-DBL_{aFLT1}) at least in the in vitro assay.

Remarkably, the covalent binding of aFLT1 on NP surface does not decrease the cytotoxicity of the transported drug but it is expected to potentiate the chemotherapeutic effect through its anti-angiogenic activity in more complex models.

In vivo anti-angiogenic potential and anticancer activity of NPs on a CAM model

Based on the promising in vitro results, we translated our investigations on MDA-MB-231 cells xenografted on CAMs. As indicated in Scheme 1, MDA-MB-231 tumors were implanted on 9-days old CAMs (E9) and the day after (E10) treatment started once a day, for a total of five days, with free DTX in DMSO

or loaded in DBL or DBL_{aFLT1} (0.083 µg DTX/day). Additional embryos were injected with the corresponding dose of empty DBL (0.83 µg/day) to exclude any cytotoxicity or effect on tumor growth caused by the vehicle.

The systemic toxicity of the different treatments on the chicken embryos was evaluated by counting the numbers of dead/surviving embryos at day 7 after beginning the treatments (E16). As shown in Fig S6, none of the treatments caused an embryos death higher than 15%, a value which was comparable with that of the negative controls (8%), namely embryos treated with PBS solution.

The anti-angiogenic effects were evaluated by counting the number of vessels arriving on the tumors on CAMs images (Figure 6A) taken on the day after the end of the treatments (E15, 6 days after tumor induction). The analysis (Figure 6B and 6C) showed that the number of vessels per tumor was significantly reduced with respect to the negative control in all the CAMs treated with DTX-loaded NPs (p values vs. negative control: 0.0077, 0.0003 and < 0.0001 for free DTX, DTX-DBL and DTX-DBL_{aFLT1}, respectively). As expected, DBL did not reduce significantly tumor angiogenesis (p= 0.8505 DBL vs. negative control).

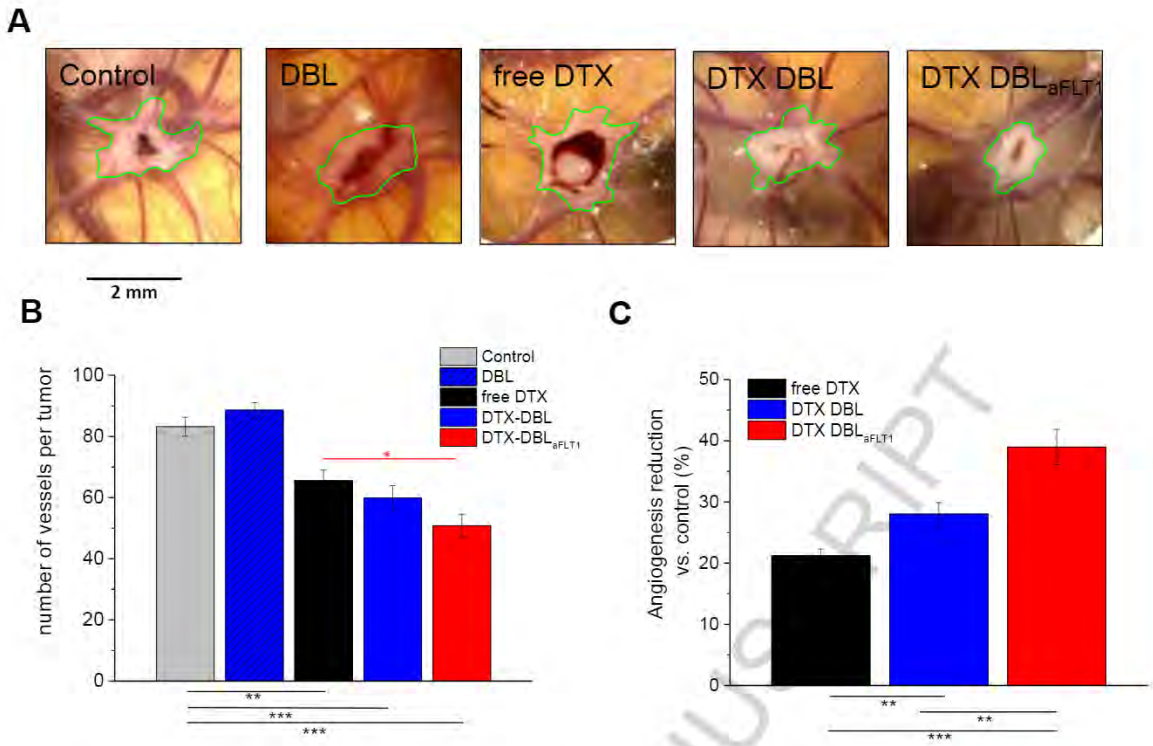

Figure 6. In vivo anti-angiogenic effects of free DTX or DTX-NPs (DTX dose 0.083 μg, NPs dose 0.83 μg) on MDA-MB-231 cells xenografted on CAMs (unloaded DBL are used as control). A) Representative images of tumors and associated blood vessels. The tumor borders are highlighted in green. B) Numbers of vessels per tumor counted on samples photographed at E15 and reported as means ± SEM for each experimental group. C) Extent of angiogenesis reduction versus negative control. * 0.05 >p value >0.01; ** 0.01 >p value>0.001; ***p value < 0.001, One-way ANOVA with post-tests.

Interestingly, DTX-DBL$_{aFLT1}$ were significantly more potent in reducing the numbers of tumor-associated blood vessels with respect to free DTX (p values of 0.0301) while DTX-DBL were not (p value of 0.7694), suggesting an important role of the anti-angiogenic aFLT1 peptide on DTX-DBL$_{aFLT1}$. Overall, the data of the counts of vessels per tumor showed that the treatments of CAMs with free DTX, DTX-DBL and DTX-DBL$_{aFLT1}$ reduced tumor angiogenesis by 21, 28 and 39%,

respectively (Figure 6B), and clearly indicated the improved efficacy of DTX nanodelivery in combination with aFLT1 peptide-based anti-angiogenic therapy with respect to the standard chemotherapy.

From the analyses of the images of tumors and associated vessels it was also evident some tumor shrinkage especially in the group treated with DTX-DBL$_{aFLT1}$ (Fig 6A).

In fact, the evaluation of the weight of the tumors removed from the CAM (E16, 7 days after tumor induction) demonstrated a significant reduction of tumor growth with all DTX formulations considered (p value < 0.001) compared to negative controls (Figure 7A).

No inhibitory effects on tumor growth were observed with DBL vs. negative control ($p = 0.336$). In agreement with the angiogenesis reduction, the most prominent effect on the inhibition of tumor growth was observed with DTX-DBL$_{aFLT1}$, followed by DTX-DBL and free DTX. The reduction of tumor weight caused by both DTX-DBL$_{aFLT1}$ and DTX-DBL was significantly higher than that of free DTX ($p < 0.01$ and $p < 0.001$, respectively) (Figure 7A). Accordingly, the percentages of tumor regression associated to CAM treatments with free DTX, DTX-DBL and DTX-DBL$_{aFLT1}$ calculated versus the negative control were 32, 46 and 60%, respectively (Figure 7B), and was significantly higher for both types of NPs with respect to free DTX ($p < 0.001$).

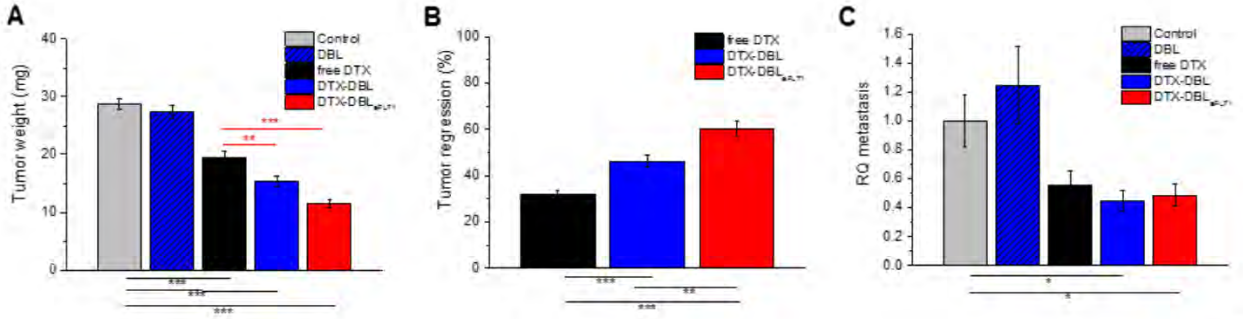

Figure 7. Tumor growth and metastasis analysis on MDA-MB-231 cells xenografted on CAMs. Tumor weight (A) and regression percentage (B) were measured by removing the tumor from normal CAM tissue on E16 and weighting them. The data are means ± SEM for each experimental group. * 0.05 >p value >0.01; ** 0.01 >p value>0.001; ***p value <0.001, One-way ANOVA with post-tests. C) Relative quantity of MDA-MB-231 metastasis (RQ). Invasion was measured by qPCR for Alu sequences in the lower part of CAMs. The arbitrary value for metastasis is 1 (negative control) and data are means ± SEM for each experimental group.

It is repeatedly reported that the neovascularization of tumors promotes the spread of cancer cells and the formation of metastasis. Thus, we assessed if the proposed anti-angiogenic NPs were able to reduce the metastatic potential of MDA-MB-231 cells xenografted on CAMs. Toward this aim, on E16 the genomic DNA of a distal portion of each CAM (lower portion) was extracted and analyzed by quantitative PCR (qPCR) with specific primers for human Alu sequences, widely recognized as a reliable method to evaluate the anti-metastatic potential of drugs in xenograft models.[46] As one can see in Figure 7C, showing the relative amount of metastatic cells, DTX NPs significantly decreased the MDA-MB-231 metastatic cells in the lower portion of the CAMs compared to negative controls (p values vs negative control: 0.0134 and 0.0388 for DTX-DBL and DTX-DBL$_{aFLT1}$, respectively). On the contrary, the metastasis reduction with free DTX was not statistically relevant (p value vs negative controls: 0.0507). The latter results did not show a positive role of aFLT1 conjugated on DBL on reducing the formation of metastases potential, at least on xenografted CAM models, but the presence of the

peptide does not have any negative effect on the overall performance of the DTX NPs ($p=0.7325$ DTX-DBL$_{aFLT1}$ vs. DTX-DBL), which was able to reduce by 50% the extent of tumor metastasis.

Conclusions

In summary, we have reported the successful preparation of NPs made of PCL-PEG copolymers conjugated with an anti FLT1 hexapeptide with anti-angiogenic properties and carrying the chemotherapeutic DTX in the internal core. The presence of the peptide on the NP surface did not interfere with the DTX loading capacity of NPs nor on their stability in biologically-relevant media as whole human plasma. The conjugation with aFLT1 imparted to NPs the ability to inhibit angiogenesis in vitro much more efficiently than the equivalent dose of free peptide, indicating that conjugation somehow strengthens the interaction of the peptide with its specific receptor VEGFR1 involved in the regulation of new vessels formation. In vitro cytotoxicity studies showed that anti-FLT1-conjugated NPs did not affect the viability of HUVEC and MDA-MB 231 cells, but they became highly cytotoxic, especially to tumor cells, when DTX is entrapped in the internal hydrophobic core. The in vitro studies did not highlight significantly higher cytotoxic effects of the DTX-loaded anti-FLT1 conjugated NPs with respect to their unconjugated counterpart or free DTX while the in vivo model of MDA-MB 231 tumor xenografted in the CAM indicated higher antitumoral effects. In fact, DTX-

loaded aFLT1 conjugated NPs induced significantly higher reduction of tumor weight and regression with respect to un-conjugated NPs and it is reasonable to assume that these effects come from the combination of improved antiangiogenic and cytotoxic activity of the NPs. Overall, the results reinforce the hypothesis that the combination of chemotherapeutics and antiangiogenic agents is a useful approach for fighting tumors and in this context a well-designed nanoplatform may represent an unprecedented tool for their combined delivery.

Author Contributions: ‖ (C.C., F.M.) These authors contributed equally. The manuscript was written through the contributions of all authors. All authors have given the approval to the final version of the manuscript. Notes The authors declare no competing financial interest.

Funding Sources

This work was supported by a grant from Regione Campania-POR Campania FESR 2014/2020 "COMBATTERE LA RESISTENZA TUMORALE: PIATTAFORMA INTEGRATE multidisciplinare per un approccio tecnologico innovativo alle oncoterapie-Campania Oncoterapie (Project N. B61G18000470007) and by Italian Association for Cancer Research (IG2014 n.15764).

REFERENCES

[1] A.M. Al-Abd, A.J. Alamoudi, A.B. Abdel-Naim, T.A. Neamatallah, O.M. Ashour, J Adv Res, 8 (2017) 591-605.

[2] L.C. Roudsari, J.L. West, Adv Drug Deliver Rev, 97 (2016) 250-259.
[3] G.C. Jayson, R. Kerbel, L.M. Ellis, A.L. Harris, Lancet, 388 (2016) 518-529.
[4] L.M. Ellis, D.J. Hicklin, Nature reviews. Cancer, 8 (2008) 579-591.
[5] G.H. Fong, J. Rossant, M. Gertsenstein, M.L. Breitman, Nature, 376 (1995) 66-70.
[6] K.H. Plate, G. Breier, B. Millauer, A. Ullrich, W. Risau, Cancer research, 53 (1993) 5822-5827.
[7] P.M. Lacal, G. Graziani, Pharmacological research, 136 (2018) 97-107.
[8] C. Fischer, M. Mazzone, B. Jonckx, P. Carmeliet, Nature reviews. Cancer, 8 (2008) 942-956.
[9] D.G. Bae, T.D. Kim, G. Li, W.H. Yoon, C.B. Chae, Clin Cancer Res, 11 (2005) 2651-2661.
[10] V.R. Elena, E.K. Jacob, G.R. Corban, B.P. Niranjan, P.T. Amir, S.P. Aleksander, Current pharmaceutical biotechnology, 12 (2011) 1101-1116.
[11] M.M. Mita, L. Sargsyan, A.C. Mita, M. Spear, Expert Opinion on Investigational Drugs, 22 (2013) 317-328.
[12] N. Ferrara, K.J. Hillan, H.P. Gerber, W. Novotny, Nature reviews. Drug discovery, 3 (2004) 391-400.
[13] G.W. Prager, M. Poettler, M. Unseld, C.C. Zielinski, Translational lung cancer research, 1 (2012) 14-25.
[14] L. Moserle, G. Jimenez-Valerio, O. Casanovas, Cancer Discov, 4 (2014) 31-41.
[15] G. Bergers, D. Hanahan, Nature reviews. Cancer, 8 (2008) 592-603.
[16] F. Collinson, M. Hutchinson, R.A. Craven, D.A. Cairns, A. Zougman, T.C. Wind, N. Gahir, M.P. Messenger, S. Jackson, D. Thompson, C. Adusei, J.A. Ledermann, G. Hall, G.C. Jayson, P.J. Selby, R.E. Banks, Clin Cancer Res, 19 (2013) 5227-5239.
[17] D. Banerjee, R. Harfouche, S. Sengupta, Vascular Cell, 3 (2011) 3.
[18] S. Mukherjee, C.R. Patra, Nanoscale, 8 (2016) 12444-12470.
[19] K. Yoncheva, G. Momekov, Expert opinion on drug delivery, 8 (2011) 1041-1056.
[20] S. Huang, K. Shao, Y. Liu, Y. Kuang, J. Li, S. An, Y. Guo, H. Ma, C. Jiang, ACS nano, 7 (2013) 2860-2871.
[21] R. Jahanban-Esfahlan, K. Seidi, B. Banimohamad-Shotorbani, A. Jahanban-Esfahlan, B. Yousefi, J Cell Physiol, 233 (2018) 2982-2992.
[22] P. Bhattarai, S. Hameed, Z. Dai, Nanoscale, 10 (2018) 5393-5423.
[23] G. Gu, Q. Hu, X. Feng, X. Gao, J. Menglin, T. Kang, D. Jiang, Q. Song, H. Chen, J. Chen, Biomaterials, 35 (2014) 8215-8226.

[24] A. Wicki, D. Witzigmann, V. Balasubramanian, J. Huwyler, Journal of Controlled Release, 200 (2015) 138-157.
[25] E. Blanco, H. Shen, M. Ferrari, Nature Biotechnology, 33 (2015) 941.
[26] I. d'Angelo, C. Conte, A. Miro, F. Quaglia, F. Ungaro, Expert opinion on drug delivery, 11 (2014) 283-297.
[27] S. Parveen, S.K. Sahoo, Journal of drug targeting, 16 (2008) 108-123.
[28] G. Shim, M.G. Kim, D. Kim, J.Y. Park, Y.K. Oh, Adv Drug Deliv Rev, 115 (2017) 57-81.
[29] S.S. Qi, J.H. Sun, H.H. Yu, S.Q. Yu, Drug delivery, 24 (2017) 1909-1926.
[30] J.A. Kemp, M.S. Shim, C.Y. Heo, Y.J. Kwon, Adv Drug Deliv Rev, 98 (2016) 3-18.
[31] Q. Hu, W. Sun, C. Wang, Z. Gu, Adv Drug Deliv Rev, 98 (2016) 19-34.
[32] P. Grossen, D. Witzigmann, S. Sieber, J. Huwyler, Journal of Controlled Release, 260 (2017) 46-60.
[33] C. Conte, I. d'Angelo, A. Miro, F. Ungaro, F. Quaglia, Current topics in medicinal chemistry, 14 (2014) 1097-1114.
[34] C. Avitabile, F. Netti, G. Orefice, M. Palmieri, N. Nocerino, G. Malgieri, L.D. D'Andrea, R. Capparelli, R. Fattorusso, A. Romanelli, Bba-Gen Subjects, 1830 (2013) 3767-3775.
[35] D.B. Endres, Clinical chemistry, 57 (2011) 815.
[36] T.D. Palmer, J. Lewis, A. Zijlstra, Journal of visualized experiments : JoVE, (2011).
[37] H.C. Kolb, K.B. Sharpless, Drug discovery today, 8 (2003) 1128-1137.
[38] T.Y. Liu, W.M. Hussein, Z.F. Jia, Z.M. Ziora, N.A.J. McMillan, M.J. Monteiro, I. Toth, M. Skwarczynski, Biomacromolecules, 14 (2013) 2798-2806.
[39] C. Conte, F. Ungaro, G. Maglio, P. Tirino, G. Siracusano, M.T. Sciortino, N. Leone, G. Palma, A. Barbieri, C. Arra, A. Mazzaglia, F. Quaglia, Journal of controlled release : official journal of the Controlled Release Society, 167 (2013) 40-52.
[40] A. Venuta, F. Moret, G. Dal Poggetto, D. Esposito, A. Fraix, C. Avitabile, F. Ungaro, M. Malinconico, S. Sortino, A. Romanelli, P. Laurienzo, E. Reddi, F. Quaglia, Eur J Pharm Sci, 111 (2018) 177-185.
[41] P. Aggarwal, J.B. Hall, C.B. McLeland, M.A. Dobrovolskaia, S.E. McNeil, Adv Drug Deliv Rev, 61 (2009) 428-437.
[42] C.C. Fleischer, C.K. Payne, Accounts of chemical research, 47 (2014) 2651-2659.

[43] M.J. Cudmore, P.W. Hewett, S. Ahmad, K.Q. Wang, M. Cai, B. Al-Ani, T. Fujisawa, B. Ma, S. Sissaoui, W. Ramma, M.R. Miller, D.E. Newby, Y. Gu, B. Barleon, H. Weich, A. Ahmed, Nature communications, 3 (2012) 972.

[44] K.A. Hotchkiss, A.W. Ashton, R. Mahmood, R.G. Russell, J.A. Sparano, E.L. Schwartz, Molecular cancer therapeutics, 1 (2002) 1191-1200.

[45] C.H. Hung, S.H. Chan, P.M. Chu, K.L. Tsai, Toxicological sciences : an official journal of the Society of Toxicology, 145 (2015) 59-67.

[46] T. Schneider, F. Osl, T. Friess, H. Stockinger, W.V. Scheuer, Clinical & experimental metastasis, 19 (2002) 571-582.

HIGHLIGHTS

- Biodegradable antiangiogenic nanoparticles made of PCL-PEG copolymers surface-decorated with an anti FLT1 hexapeptide for the delivery of docetaxel have been developed.
- Nanoparticles entrap docetaxel with high efficiency and sustained its release along time in simulated biological conditions.
- aFLT1-decorated nanoparticles inhibit angiogenesis in vitro much more efficiently than the equivalent dose of free peptide and docetaxel.
- In an in embryo model of breast cancer, docetaxel-loaded aFLT1-decorated nanoparticles reduce significantly tumor mass as compared with free drug due to combined antiangiogenic and cytotoxic effects.